Research Article

WIND ENGINEERING

A wind tunnel investigation of yawed wind turbine wake impacts on downwind wind turbine performances and wind loads

Takanori Uchida[1] [ID], Koichiro Shibuya[2], Gustavo Richmond-Navarro[3] [ID] and Williams R. Calderón-Muñoz[4,5]

Abstract

In the current work we experimentally explored yawed wind turbine wake impacts on downwind wind turbine performances and wind loads. The lab-scale wind turbine model with a rotor diameter (D) of 0.442 m and a height of 1 m (=2.26D) was installed in a closed-circuit boundary layer wind tunnel (test section: 15 m long × 3.6 m wide × 2.0 m high) of the Research Institute for Applied Mechanics (RIAM) of Kyushu University. Power performance tests were initially conducted with a single rotor in isolation in order to characterize a rotor's power output in stand-alone conditions. A detailed comparison of the tests revealed that the power output decreased rapidly as the yaw angle (γ) increased. It is presumed that the power output decrease in yawed cases is mainly due to the decrease in the effective rotor area and the change in the angle of the incoming wind flow with respect to the wind turbine blade. Next, using two wind turbine models aligned with the dominant inflow direction, the merging wakes behaviors caused by three different lateral separation distances were tested: (a) Case 1 ($y = 0$), (b) Case 2 ($y = 0.5D$), and (c) Case 3 ($y = 1D$). Here, the separation distance between the two wind turbine models was fixed at 6D in all cases. Extremely large power output deficits of 46%–76% were seen in the Case 1 configuration. This is mainly due to the significant wake velocity deficits induced by the upwind wind turbine model. In the Case 2 configuration with γ values of 20° and 30°, a significant increase in the power output of the downwind wind turbines was observed. Similar to Case 1 configuration, these results are considered to be mainly due to the upwind turbine-induced wake velocity deficits and wake deflection. Finally, in the Case 3 configuration, no significant difference was found in all of the results, and the tendency was almost the same. We show that the wake velocity deficits induced by the upwind wind turbine model had almost no effect on the power output of the downwind wind turbine model. We evaluated the total power output of the two turbines. As a result, in the Case 2 configuration with 20° yaw angle, the total power output of the two wind turbine models was the highest due to the increase in the power output of the downwind wind turbine model. In order to investigate the main cause of the significant increase in the power output of the downwind wind turbine model at 20° and 30° yaw angles in the Case 2 configuration, we measured the lateral wind speed distribution at the 6D position on the downwind side of the upwind wind turbine model by using the ultrasonic anemometer. As a results, it was clarified that the peak of the wake velocity deficits induced by the upwind wind turbine model is clearly shifted away from the downwind turbine such that it experiences a smaller deficit due to wake steering. Also, with wake steering the upwind turbine-induced wake velocity deficits may be smaller due to the reduction in rotor area. Finally, it is extremely important to understand the wind load acting on the downwind wind turbine model operating within the wake region induced by the upwind yawed wind turbine model when the maximum power output is generated. It can be seen that as the yaw angle of the upwind wind turbine model increased, the power output generated by the downwind wind turbine model and the streamwise wind load acting on it also increased. However, it was also clarified that the streamwise wind load acting on the downwind wind turbine model in this situation did not exceed the stand-alone value.

[1]Research Institute for Applied Mechanics (RIAM), Kyushu University, Kasuga, Fukuoka, Japan
[2]Engineering and Technology Development Department, Wind Power Business Unit, Hitachi Zosen Corporation, Suminoe-ku, Osaka, Japan
[3]Department of Electromechanical Engineering, Instituto Tecnológico de Costa Rica, Cartago, Costa Rica
[4]Department of Mechanical Engineering, Faculty of Physical and Mathematical Sciences, Universidad de Chile, Santiago, Chile
[5]Energy Center, Universidad de Chile, Santiago, Chile

Corresponding author:
Takanori Uchida, Research Institute for Applied Mechanics (RIAM), Kyushu University, 6-1 Kasuga-kouen, Kasuga, Fukuoka 816-8580, Japan.
Email: takanori@riam.kyushu-u.ac.jp

Introduction

The Government of Japan has set a high goal of reducing greenhouse gas emissions by 46% from 2013 levels by 2030 and reaching virtually zero (carbon neutral) by 2050. In Japan, even though wind power generation, and especially offshore wind power generation, only constitutes a small part of the total power source, offshore wind power generation is expected to develop rapidly in the near future. The potential offshore market is the main driver today for the development of large wind turbines and many other related tasks.

Solitary wind turbines traditionally produce the most power when pointing directly into the wind. In addition, wind turbine operation induces a downwind decrease in wind speed and an increase in turbulence intensity in the form of a wake. Generally speaking, wind turbines located offshore are always clustered in wind farms in order to limit the overall installation and maintenance expenses and transmission line constraints. When tightly packed lines of turbines face the wind on wind farms, it has been pointed out that wake interference among upwind and downwind wind turbines often occurs. In other words, the wakes of upwind wind turbines negatively affect downwind wind turbines. When wake interference in wind farms occurs, partial wakes from upwind wind turbines overlap with a part of the wakes of downwind wind turbines. Accordingly, wind turbines operating in the wake of upwind turbines experience wake-induced power losses and increased mechanical fatigue loads due to high turbulence from upwind turbine wake effects. Wake effects from adjacent wind turbines, termed wake mixing, lead to changes in ambient wind field conditions that alter the dynamic loading on the downwind turbines.

In order to increase overall wind farm power production and also significantly extend the lifetime of the turbine through reduced mechanical fatigue damage (structural loading), some wind power plant-wide control strategies enhance the overall wind farm energy production while reducing the mechanical fatigue damage on wind turbines have been proposed. Among some proposed methods, recently, the yaw-based wake steering has been shown to be a promising concept of wind farm control (He, 2022; Houck, 2022; Kheirabadi et al., 2019; Porté-Agel et al., 2020). This approach maximizes overall wind farm power production through yaw misalignment, which deflects wakes away from downwind turbines, and prolongs the lifetime of the turbines through reduced fatigue damage. In wake steering technology, yawing the rotors of the upwind wind turbines causes a shift in the direction of the wind turbine wake away from downwind wind turbines. As a result, two things happen: the power production of the yawed wind turbines decreases because the effective rotor area affected by the incoming wind flow becomes smaller, and the wakes behind these turbines are redirected aside from the downwind wind turbines.

According to the latest research, Howland et al. (2019) designed a wake steering control scheme to increase the power production of wind farms with site-specific analytic gradient ascents relying on historical operational data. The wake steering protocol was applied to an operational wind farm consisting of an array of six utility-scale turbines located in Alberta, Canada. As a result, it was shown that it increased the power production for wind speeds near the site's annual average between 7% and 13% and decreased variability by up to 72% for selected wind directions at night. These improvements can contribute to increasing the ability of wind farms to provide reliable, low-cost, and efficient base energy load. Bensason et al. (2021), working at the US Department of Energy's National Renewable Energy Laboratory (NREL), illustrated how wake steering can increase energy production for a large sampling of commercial land-based US wind power plants. While some plants showed less potential for wake steering due to unfavorable meteorological conditions or turbine layout, several wind power plants were ideal candidates that could benefit greatly from wake steering control. Overall, a predicted average Annual Energy Production (AEP) gain of 0.8% was found for the set of wind plants investigated. In addition, the researchers found that on wind plants using wake steering, wind turbines could be placed more closely together, increasing the amount of power produced in a given area by nearly 70% while maintaining the same cost of energy generation. Other research related to wake steering has already been reported from wind tunnel experiments (Bartl et al., 2018; Campagnolo et al., 2020; Richmond-Navarro et al., 2021; Schottler et al., 2018), analytical modeling (Qian et al., 2018; Wei et al., 2021), numerical simulations (Lin et al., 2019; Miao et al., 2016), and field observations (Brugger et al., 2020; Fleming et al., 2017).
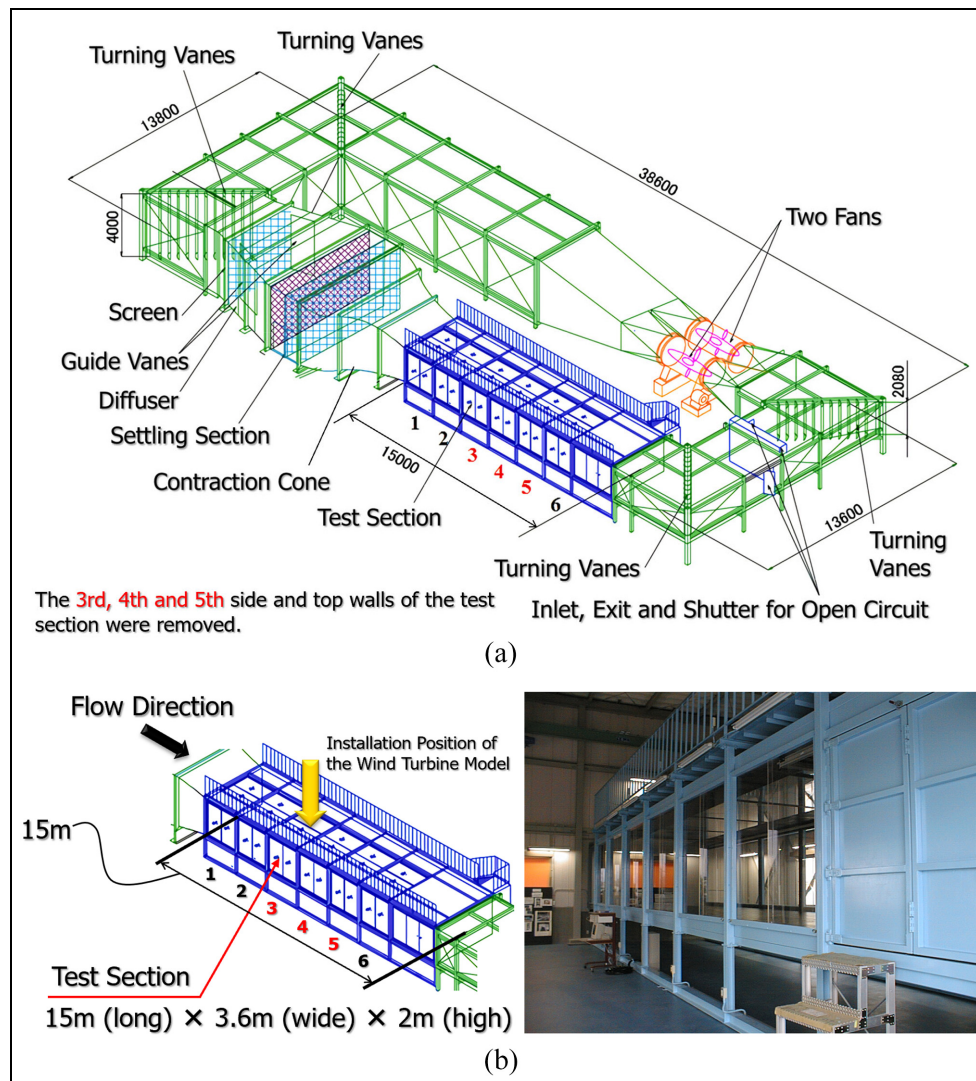
Because of the uncertainty due to the complexity of wake dynamics, it is extremely important to understand the flow characteristics of the yawed wind turbine wakes in detail in order to improve the accuracy of wake steering. Depending on complex turbulent, thermally-driven atmospheric conditions, where wind speed and air temperature vary with height and location, all utility-scale wind turbines often operate in far from ideal conditions. Therefore,

all utility-scale wind turbines are always yawed in reality. It should be noted here that the definition of "yawed" used in the current study is that a wind turbine model is misaligned with the dominant inflow direction.

In this paper, we experimentally evaluated yawed wind turbine wake impacts on downwind wind turbine performances and wind loads. The merging wakes behaviors caused by three different lateral separation distances were tested using two aligned wind turbine models with a rotor diameter (*D*) of 0.442 m and a height of 1 m (= 2.26*D*).

Description of experimental equipment

We will first present an overview of the wind tunnel equipment used. Wind tunnels are classified into two main types: open-circuit and closed-circuit. In an open-circuit tunnel, the airflow follows a straight path from the entrance through a contraction zone to the test section, and then moves into a diffuser, a fan section, and an outlet. In a closed-circuit wind tunnel, the air recirculates continuously with little or no exchange with the outside. The wind tunnel facility used in this study is a closed-circuit boundary layer wind tunnel (test section: 15 m long × 3.6 m wide × 2.0 m high) of the Research Institute for Applied Mechanics (RIAM) of Kyushu University. Figure 1(a) presents an overall view of the facility, whereas Figure 1(b) presents an enlarged view of the test section and the sidewall of the wind tunnel, looking in the upwind direction. The blockage ratio of the swept area of the wind turbine model used in the current study to the cross-sectional area of the wind tunnel is about 2%, which is sufficiently small. The current authors confirmed in advance that the initial wake expansion of an isolated rotor will not be greatly affected by the presence or absence of the third, fourth, and fifth side and top walls.

Figure 1. Closed-circuit wind tunnel facility used in this study: (a) perspective view and (b) enlarged view of the test section and photo of the sidewall of the wind tunnel.

Experimental set-up and small-scale wind turbine model

Figure 2 shows a schematic view of the torque-measurement system used in the performance test of the small-scale wind turbine model we produced. Figure 2 also specifies various parameters of the performance test. As shown in Figure 2, the inflow wind speed (U_{in}) was set to 15 m/s in the wind tunnel experiment. In this study, we did not consider the scaled boundary layer that is generally created in the wind tunnel using triangular spires and distributed roughness elements. In this study, we set a uniform flow in which the wind speed does not change in the vertical direction. The details will be described later, but the height of the wind turbine model used in this study was 1 m, and the rotor diameter (D) was 0.442 m. The Reynolds number $Re = U_{in}D/\nu$ determined for a rotor diameter D was in the order of 10^5, where ν is the kinematic viscosity of the fluid. The voltage output from the torque meter attached to the wind turbine model shown in Figure 2 was low-pass filtered at 1 Hz and was recorded at 1 kHz for 30 seconds and subsequently averaged. Detailed studies performed with this facility have been published in the literature. Notably, Richmond-Navarro et al. (2021) studied the shrouded wind turbine performance in yawed turbulent flow conditions.

In this study, we prepared two types of three-bladed, fixed-pitch, small-scale wind turbine models. Note that a current lab-scale wind turbine model was designed to study its wind turbine aerodynamics generated in the wind tunnel. Therefore, scaling of utility-scale wind turbine rotor in reality is not considered (Li et al., 2020). One is the small-scale wind turbine model designed for performance testing as shown in Figure 3. From now on, for convenience, we will call it the Type-A model. Figure 3 shows a photograph of a 30° yaw angle. Furthermore, the torque meter and servo motor used in this study are also shown in Figure 3. Another model is a compact type small-scale wind turbine model that can control only rotor rotation speed as shown in Figure 4. From now on, for convenience, we will call it the Type-B model. As shown in Figure 4(b), there is no torque meter to that shown in Figure 3(b); only the same servo motor shown in Figure 3(b) is stored in the box corresponding to the nacelle.

Figure 5 shows a small-scale wind turbine blade used for the present study. The same wind turbine blade shown in Figure 5 was used in both Type-A and Type-B models (see Figures 3 and 4). The blades of the small-scale wind turbine model are based on the airfoils designed by Matsumiya et al. (2011). As mentioned earlier, the blade diameter (rotor diameter) used in this study was $D = 0.442$ m. Figure 6 shows a cross-section of each region from root to tip of the blade. The gravity center position is also specified in this figure. Figure 7 shows a variation of the chord length and the twist angle from the root to the tip of the blade. Figure 8 shows the lift coefficient CL and drag coefficient CD against the angle of attack in the blade cross-section at the 75% position from the rotor center.
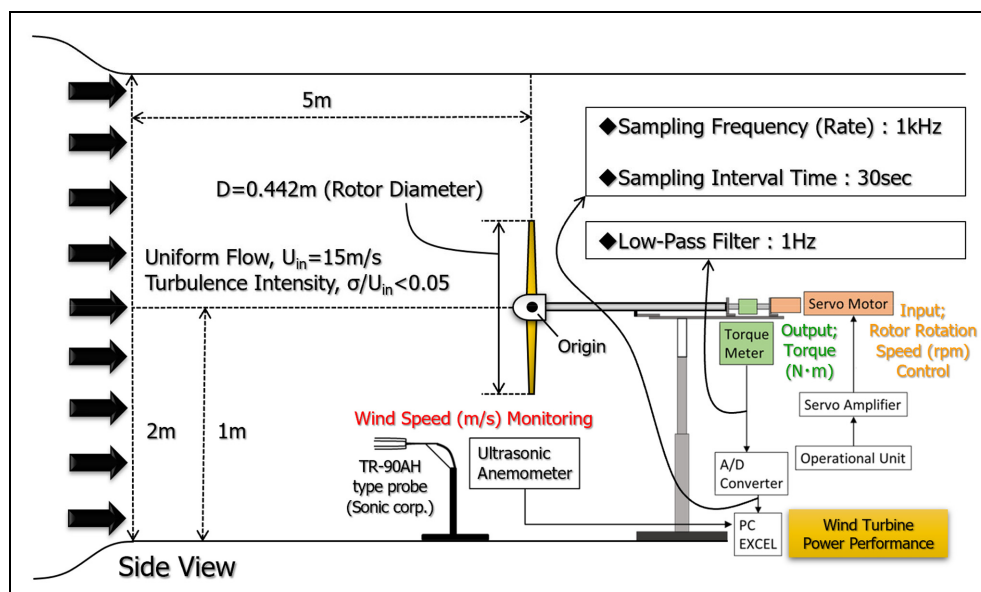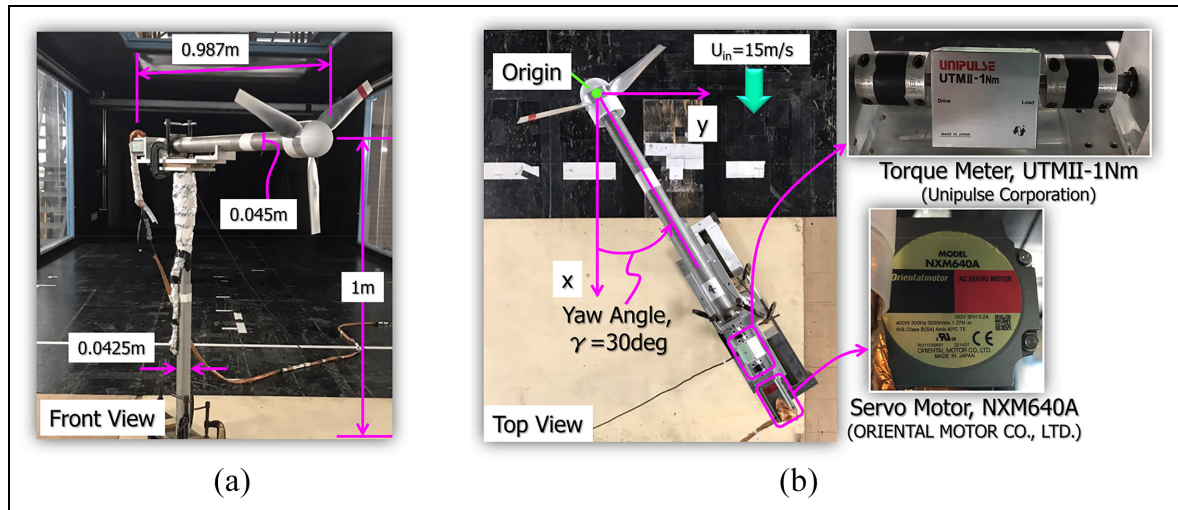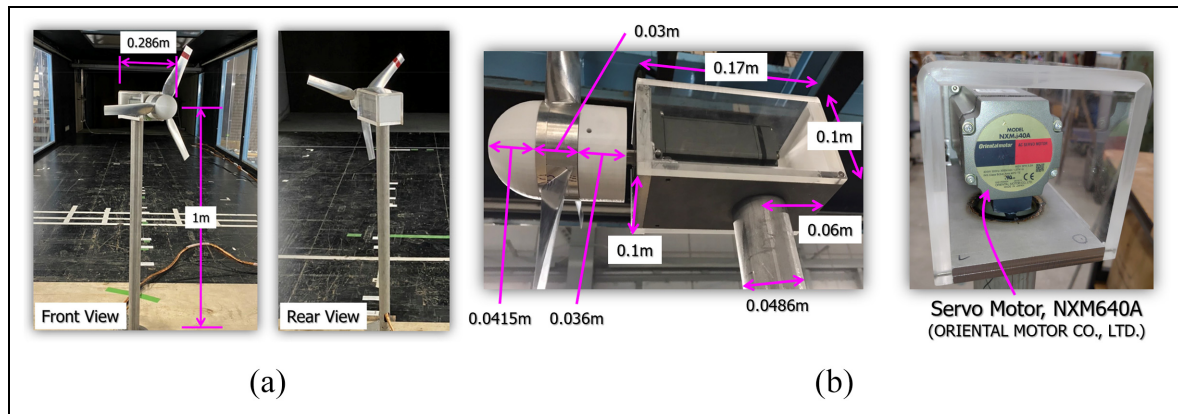

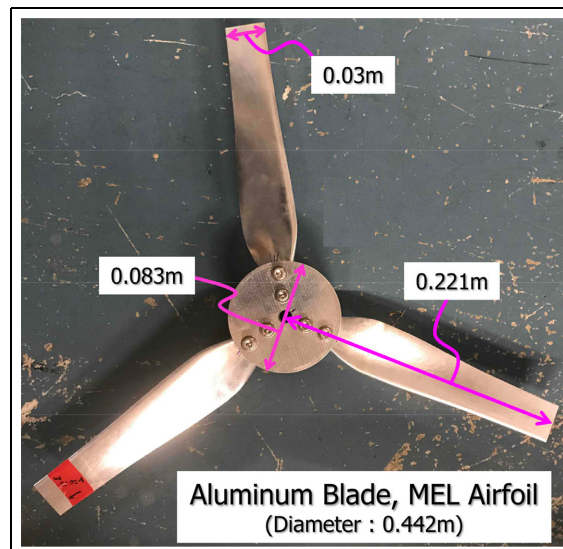**Figure 2.** Schematic view of the torque-measurement system used in the performance test.

Figure 3. Wind turbine model (Type-A model) used for the performance test: (a) front view and (b) top view.

Figure 4. Wind turbine model (Type-B model) that can control only rotor rotation speed: (a) overall view and (b) enlarged view.

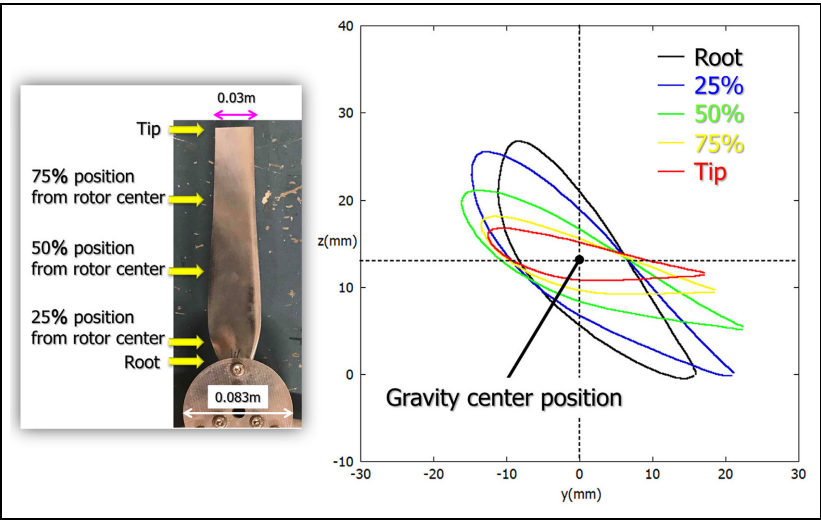**Figure 5.** Wind turbine blade used for the Type-A and the Type-B models.

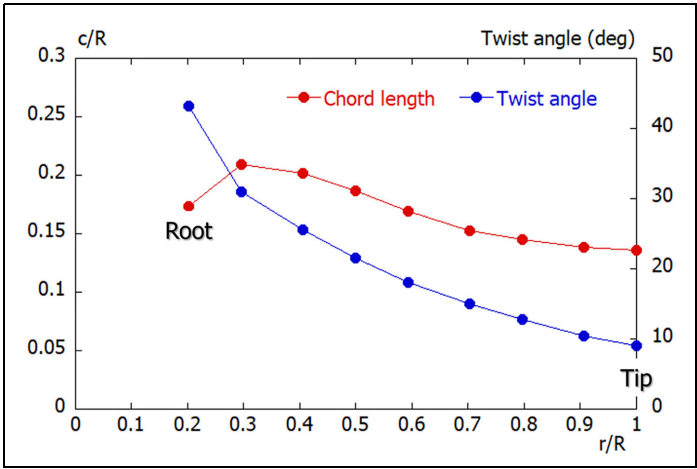**Figure 6.** Cross-section of each region from root to tip of the blade.

Figure 7. Variation of the chord length and the twist angle from the root to the tip of the blade.
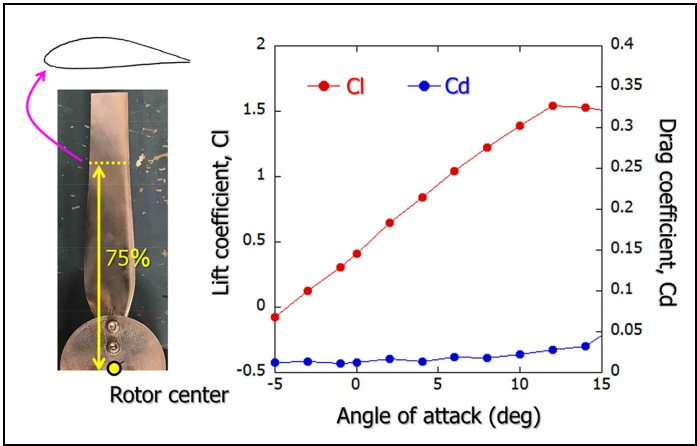

Figure 8. Lift coefficient and drag coefficient against angle of attack in the blade cross-section at the 75% position from the rotor center.
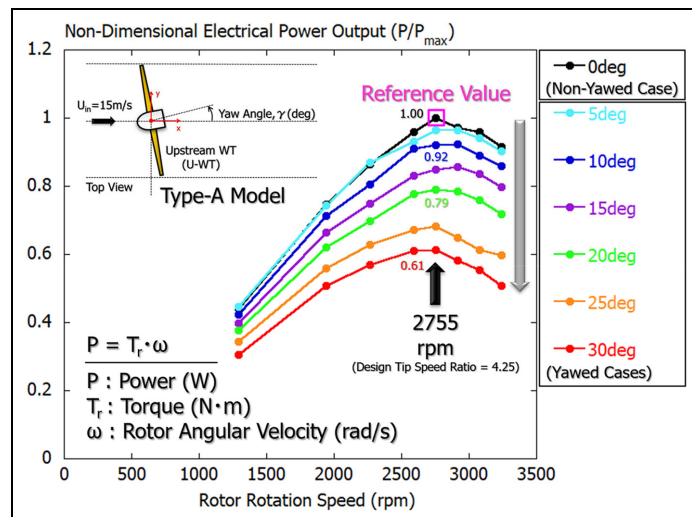
Power performance under yawed conditions for one small-scale wind turbine model

Prior to conducting multi-rotor experiments in the wind tunnel, power performance tests were initially conducted with a single rotor in isolation in order to characterize a rotor's power output in stand-alone conditions using only Type-A model (see Figures 2 and 3). The current measurements were repeated at least two to three times on different days and quantify the uncertainty in them. As a result, almost identical results were obtained without the need to draw error bars. Multi-rotor experiments were subsequently conducted using two types of wind turbine models, Type-A and Type-B models (see next section).
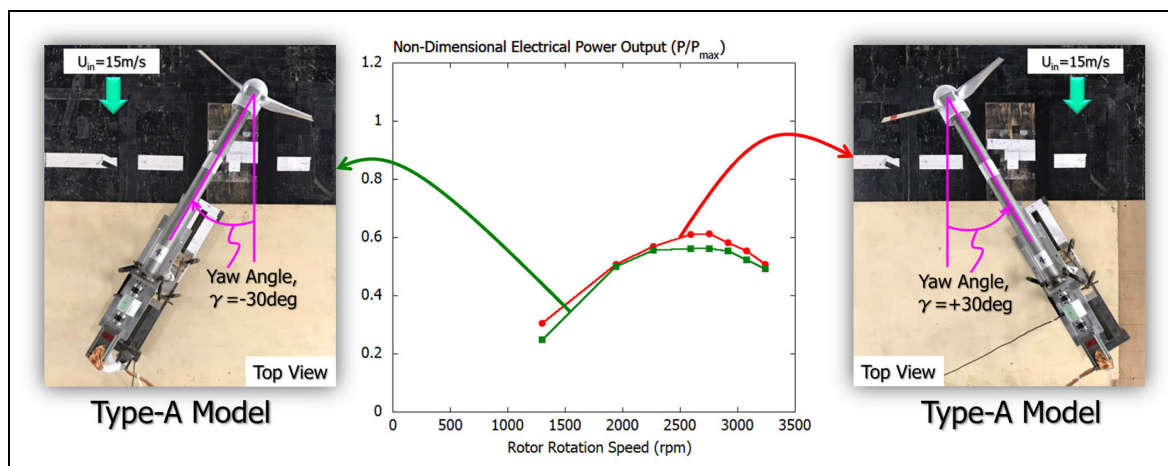
In the first experiment, we obtained data for a total of seven cases with 0° yaw angle (non-yawed case) and yaw angles of 5°, 10°, 15°, 20°, 25°, and 30° (yawed cases), and compared them. Figure 9 shows the graph of the obtained experimental results. In Figure 9, the horizontal axis shows the rotor rotation speed (rpm). In particular, to clarify differences and trends in measurement results, the vertical axis shows the non-dimensional electrical power output. Furthermore, for the non-dimensional electrical power output shown on the vertical axis, the maximum value of the non-yawed case was used as the reference value, and all other numerical values were normalized using this value. A detailed observation of Figure 9 revealed that the corresponding non-dimensional power output decreased rapidly as the yaw angle increased. Here, we also found that the rotor rotation speed at which the maximum power output can be obtained in each case was almost the same at 2755 rpm. In the non-yawed case, the tip speed ratio derived from this 2755 rpm was 4.25, as shown in Figure 9. It is presumed that the reason why the power output decreased in yawed cases is mainly the decrease in the effective rotor area and the change in the angle of the incoming wind flow with respect to the wind turbine blade. In addition, with wake steering the wake velocity deficits may be smaller due to the reduction in rotor area and so a reduced overall thrust force on own wind turbine model.

In this study, to examine the effect of own positive and negative yaw misalignment on own turbine performance, we also compared the non-dimensional electrical power output at yaw angle ± 30°. The obtained experimental results are shown in Figure 10. Through the comparison of the results shown in Figure 10, it was clarified that there was no significant difference between the experimental results of both cases.
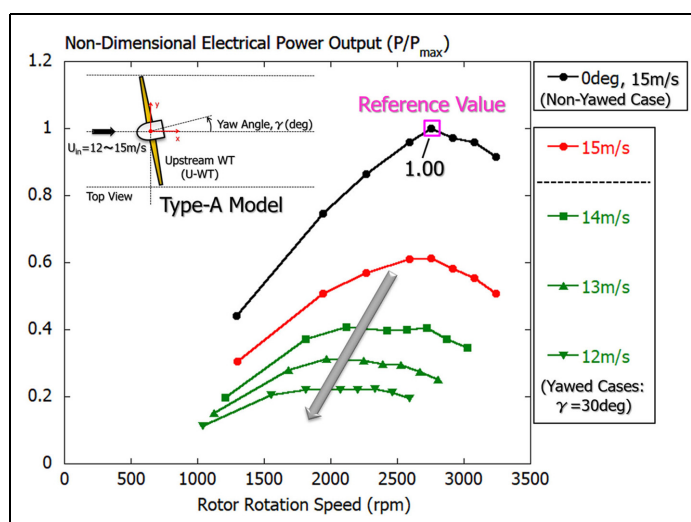
Furthermore, in the yawed case with yaw angle + 30°, a parametric study was conducted with four different incoming wind speeds. Specifically, the effect of incoming wind speed on power output was also examined. The obtained results are shown in Figure 11. As expected, we found that the power output also decreased as the incoming flow speed decreased, and the rotor rotation speed, which indicates the maximum value, also decreased.

Figure 9. Non-dimensional electrical power output under yawed conditions for one wind turbine model (Type-A model).

Figure 10. Non-dimensional electrical power output at yaw angle $\pm 30°$ for one wind turbine model (Type-A model).

Figure 11. Non-dimensional electrical power output at yaw angle $+ 30°$ for one wind turbine model (Type-A model) when inflow wind speed is changed.

Power performance under yawed conditions for two small-scale wind turbine models

In the current experimental study, as shown in Figure 12, three different cases of merging wake were set and the impact of yawed wind turbine wake on the performance of the downwind wind turbine model was investigated in detail. In the current section, the Type-B model shown in Figure 4 was used for the upwind wind turbine, and the Type-A model shown in Figure 4 was used for the downwind wind turbine to evaluate the power output. The spacing between the upwind and the downwind wind turbine models was set to six times the diameter of the rotor (D). The yaw angle of the upwind wind turbine model was rotated in the positive direction up to a range of 30°. Similar to the wind tunnel experiments described so far, the inflow wind speed (U_{in}) was set to 15 m/s.

Figure 13 shows the non-dimensional electrical power output of the downwind wind turbine model when the upwind wind turbine model was in the yawed conditions. First, let us focus on the experimental results obtained in the Case 1 shown in Figure 13(a). A number of full-scale offshore wind farms have a regular, grid-like, design, in which power losses due to the longitudinal alignment of turbines can be significant. According to previous wind farm performance studies, the power output from turbines in the second row of

a wind farm with downwind separation of $7D$–$10D$ has been shown to be 40% and 20% lower, respectively, than the power output of the upwind wind turbines (Barthelmie et al., 2010). An extremely large reduction in power output was seen in the current scaled wind tunnel experiments with a $6D$ downwind separation distance between wind turbine models aligned with the dominant inflow direction. This is mainly due to the significant wake velocity deficits induced by the upwind wind turbine model and wake deflection. Focusing on the arrangements of yaw angles 0° and 10°, the downwind wind turbines resulted in power output deficits of 75%–76%, compared to a single wind turbine in isolation at the downwind wind turbine position (reference value). In the experimental results where the yaw angle was in the range of 20°–0°, the power output of the downwind wind turbines was significantly increased compared to γ values of 0° and 10°. In these two cases, a power deficit of 46%–60% was clearly observed.

Next, let us focus on the experimental results obtained in the Case 2 shown in Figure 13(b). In these arrangements, the power output of the downwind wind turbines showed an increasing tendency as a whole compared to the experimental results of the aligned wakes shown in Figure 13(a). What is particularly noteworthy here is that significant increases in the power output of the downwind wind turbines in the case of γ values of 20° and 30° were observed. This result is considered to be mainly due to the upwind turbine-induced wake velocity deficits and wake deflection.

Finally, we consider the experimental results obtained in the Case 3 shown in Figure 13(c). In this configuration, no significant difference was found in all the results, and the tendency was almost the same. We found that the wake velocity deficits induced by the upwind wind turbine model and wake deflection had almost no effect on the power output of the downwind wind turbine model.
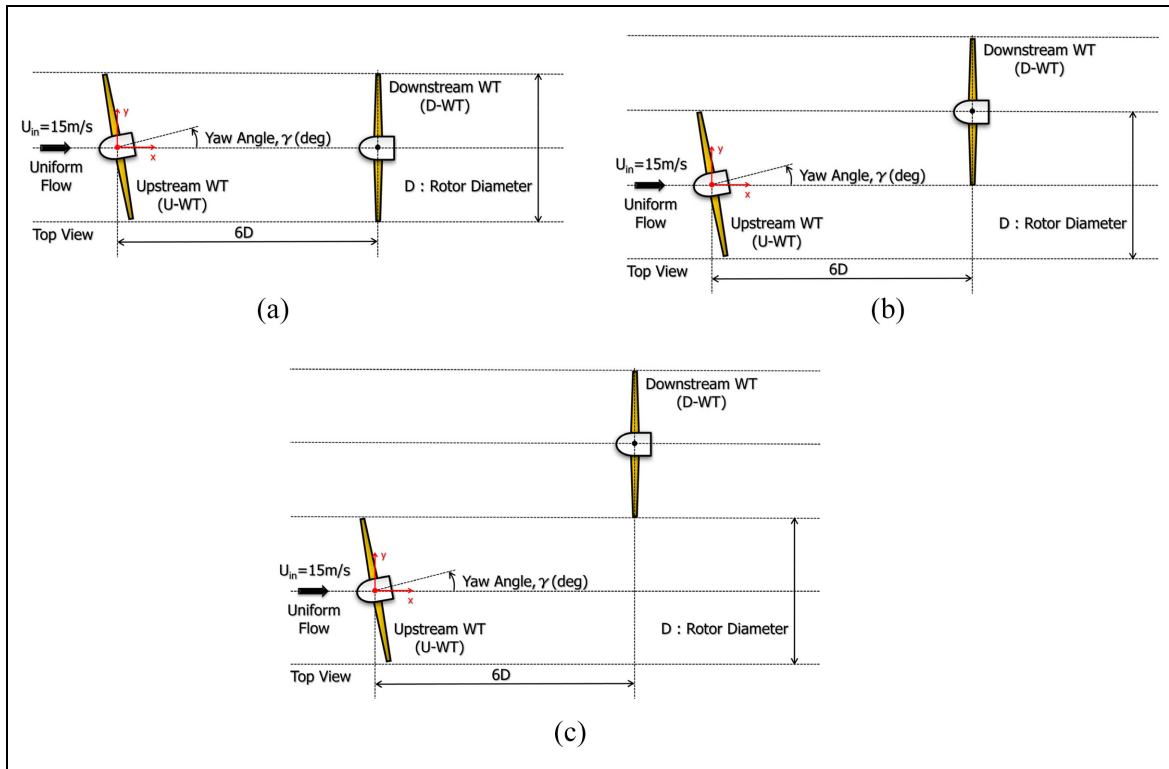
We extracted the maximum value of power output from the experimental results of the wind turbine alone shown in Figure 9, the experimental results in the Case 1 shown in Figure 13(a), and the experimental results in the Case 2 shown in Figure 13(b). Based on the maximum power output in these different cases, we created the bar graph shown in Figure 14. In other words, Figure 14 shows the maximum power output of the upwind and the downwind wind turbine models in the Case 1 and the Case 2. Through careful observation of the results shown in Figure 14, the power output of the upwind wind turbine model decreased as the yaw angle of the upwind wind turbine model increased.

The current configurations shown in Figure 12(a) and (b) are considered as a mini wind farm consisting of two wind turbine models. Furthermore, we integrated the power outputs of the upwind and the downwind wind turbine models and display them as the total power outputs in Figure 15. Of course, the experimental results in the Case 2 shown in Figure 15(b) are better than the experimental results in the Case 1 shown in Figure 15(a). What should be particularly emphasized in Figure 15(b) is that when the yaw angle equaled 20°, the total power output of the two wind turbine models was the highest due to the increase in the power output of the downwind wind turbine model. That is, the above experimental result demonstrated a current wake steering effect when the upwind turbine model was yawed, and although the upwind turbine model is expected to lose power by being yawed, the net power output can go up based on the increased power of downwind turbine model now out of the wake.
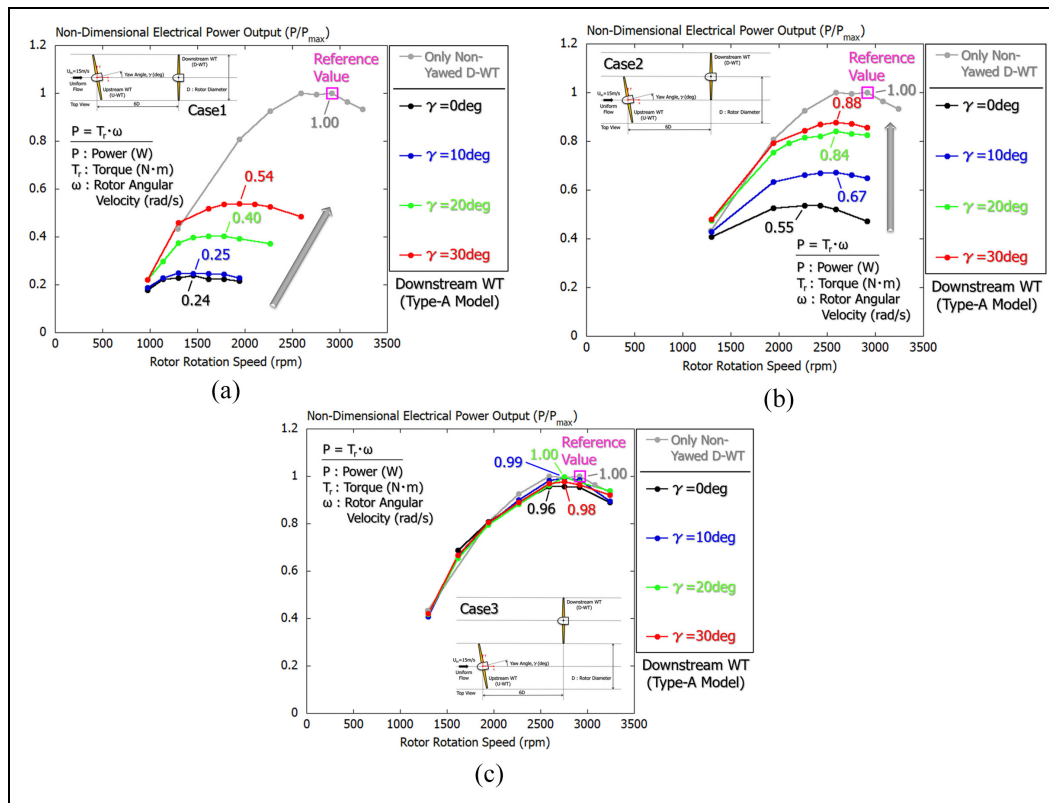
In order to consider the main cause of the significant increase in the power output of the downwind wind turbine model at the yaw angles of 20° and 30° in the Case 2 shown in Figure 12(b), we measured the lateral wind speed distribution at the $6D$ position on the downwind side of the upwind wind turbine model by using an ultrasonic anemometer (Sonic corporation DA-700 with TR-90AH type probe, Processing accuracy; within 1%, Resolution; 0.005 m/s), as shown in Figure 16. In the current experiment, we programmed it to perform automatic experiments with probe traversing and data acquisition. The obtained airflow measurement results are shown in Figure 17 together with the wind turbine configuration.

Let us focus on the experimental result of yaw angle 20° displayed with the green symbol and line and the experimental result of yaw angle 30° displayed with the red symbol and line. Through careful observation of the results shown in Figure 17, it was clarified that the peak of the wake velocity deficits induced by the upwind wind turbine model is clearly shifted away from the downwind turbine such that it experiences a smaller deficit due to wake steering. Also, it was also clarified that the inclined flow due to deflection of the wake from the upwind wind turbine model was formed as shown by the gray arrow in Figure 17. It can also be seen that the inclined angle gradually increased as the yaw angle increased.
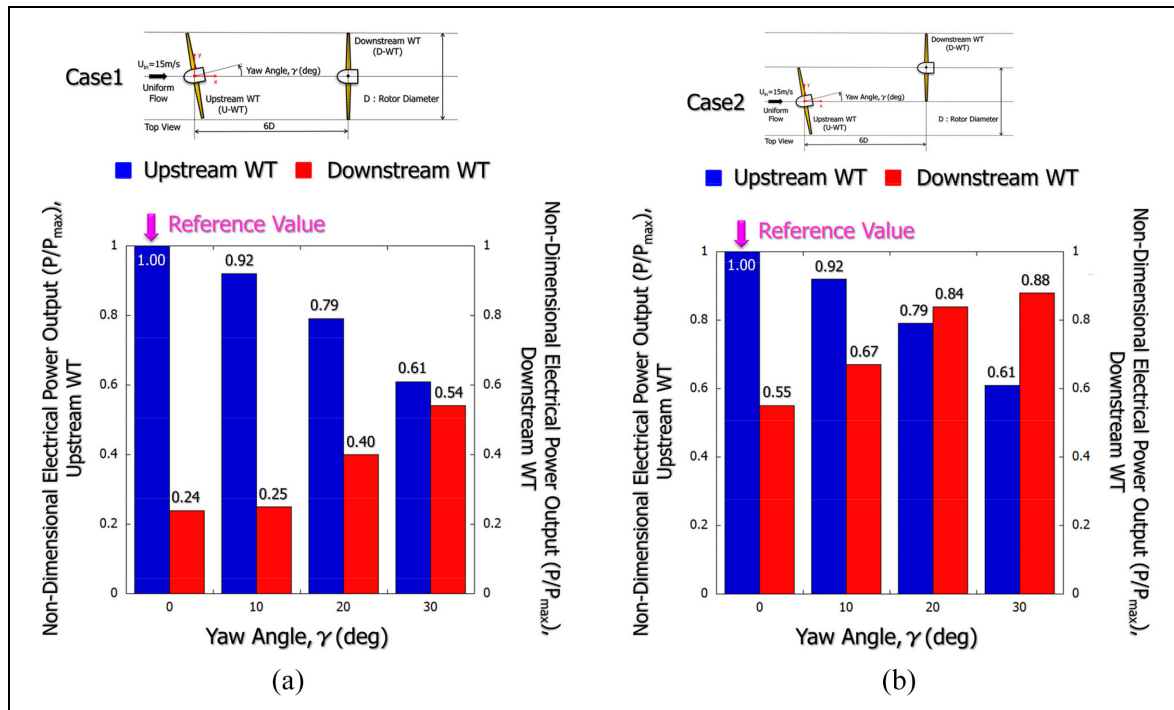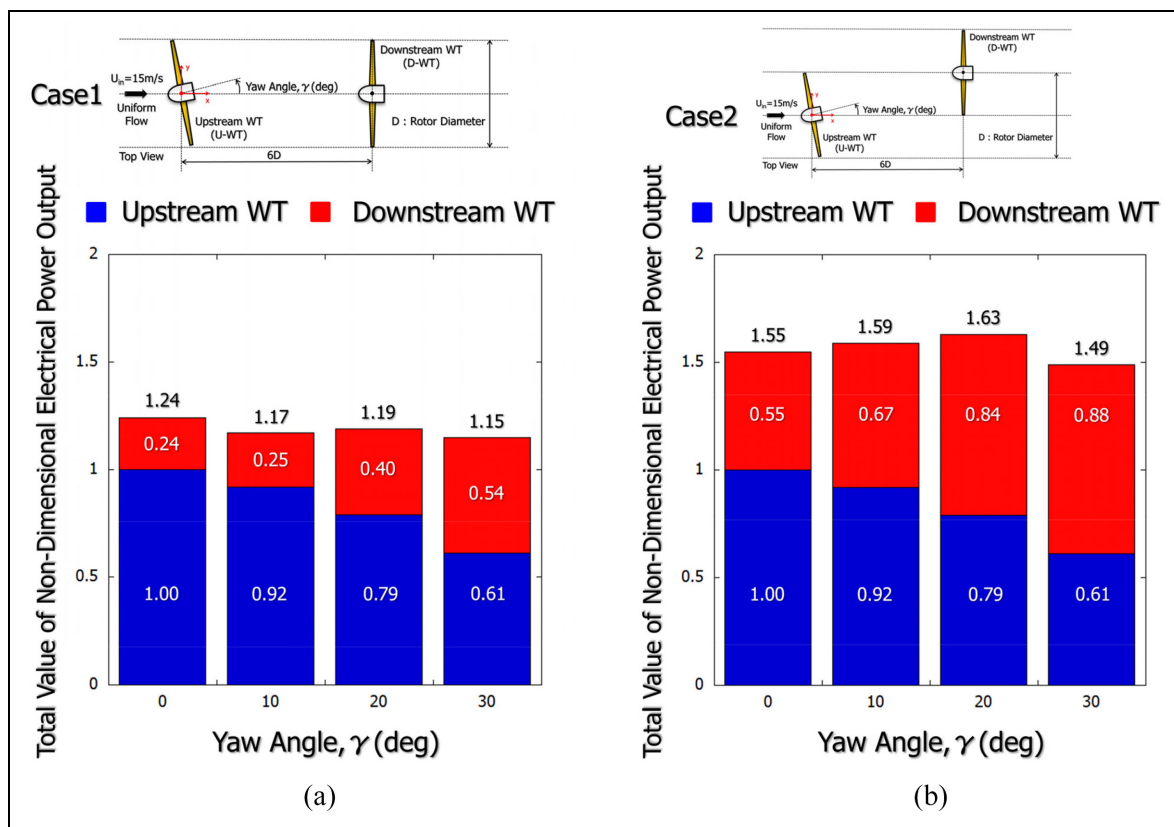
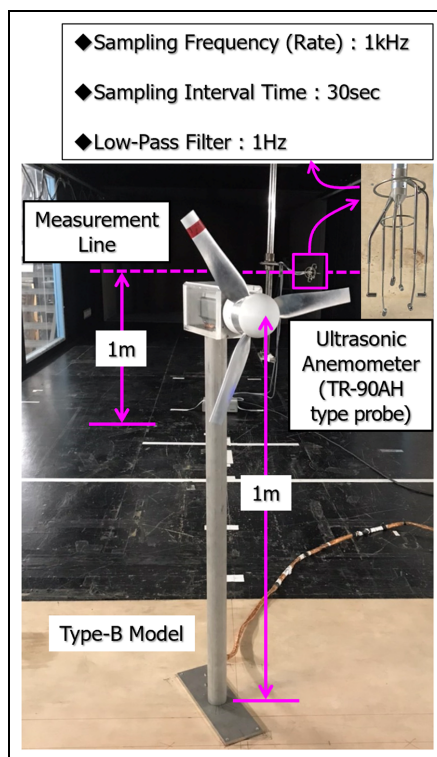**Figure 12.** Three different cases of merging wakes: (a) Case 1 (*y* = 0), (b) Case 2 (*y* = 0.5*D*), and (c) Case 3 (*y* = 1*D*).

Figure 13. Non-dimensional electrical power output under yawed conditions for two wind turbine models: (a) Case1 (*y* = 0), (b) Case2 (*y* = 0.5D), and (c) Case3 (*y* = 1D). Here, the Type-B model was used for the upwind wind turbine, and the Type-A model was used for the downwind wind turbine.
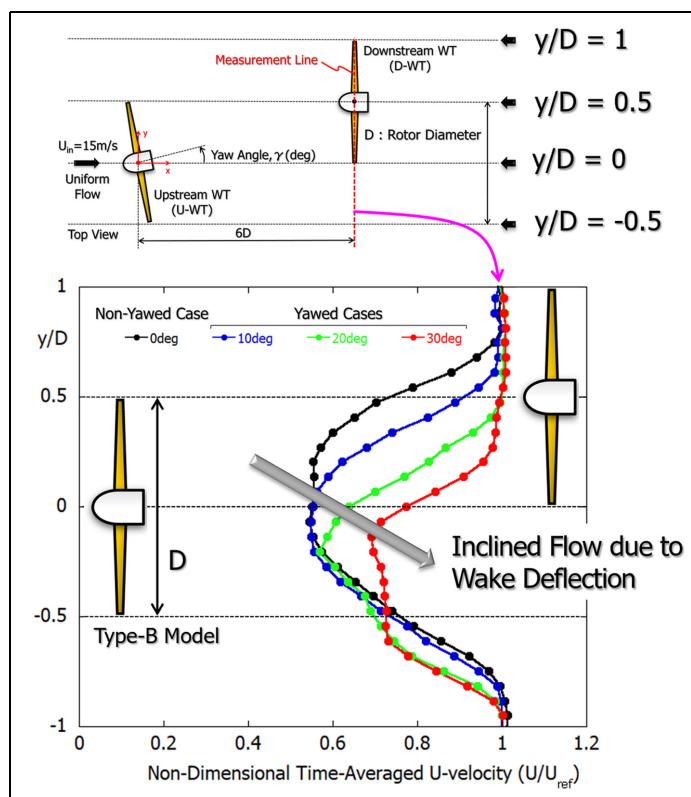
Figure 14. Maximum power output of the upwind and the downwind wind turbine models: (a) Case 1 and (b) Case 2 using the Type-A model.

Figure 15. Total power output of the upwind and the downwind wind turbine models: (a) Case 1 and (b) Case 2 using the Type-A model.

Figure 16. Measurement of lateral wind speed distribution downwind of the Type-B model using an ultrasonic anemometer.
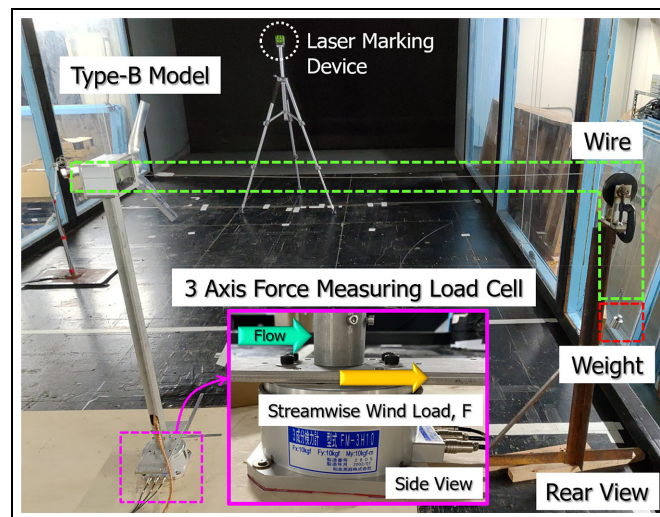

Figure 17. Lateral mean wind speed distribution at 6*D* downwind position (hub height; 2.26*D*) of upwind wind turbine model (Type-B model).
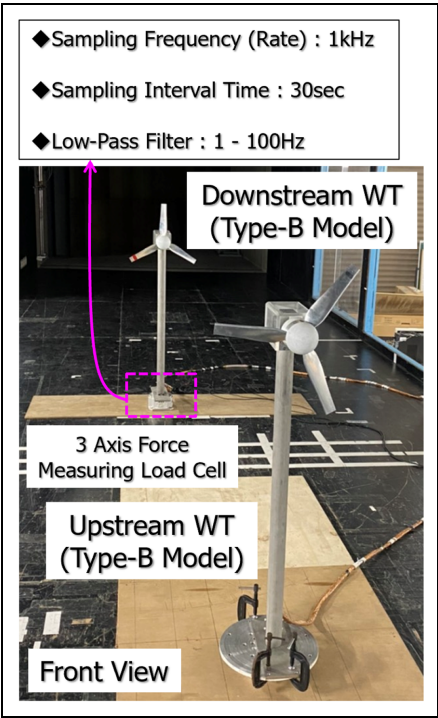
Wind load under yawed conditions for two small-scale wind turbine models

It is extremely important to understand the wind load acting on the downwind wind turbine model operating within the wake region induced by the upwind yawed wind turbine model when the maximum power output was generated. Therefore, in the current experimental study, the downwind wind turbine model was mounted on a three-axis force measuring load cell (capacity: Fx; 10kgf, Fy; 10kgf, My; 10kgf-m), and the streamwise wind load acting on the downwind turbine model was measured in the Case 2 (see Figures 18 and 19). The output signals produced by a load cell are mostly small. Therefore, a load cell amplifier converting the small signal into more powerful voltage signals was used. Basically, in the current experiment voltage signals from the load cell were off-set, amplified, and then digitized using an analog-digital converter on a personal computer, at a sampling frequency of 1 kHz per channel (filter cutoff frequency 1–100 Hz). The typical duration of each record was about 30 seconds.
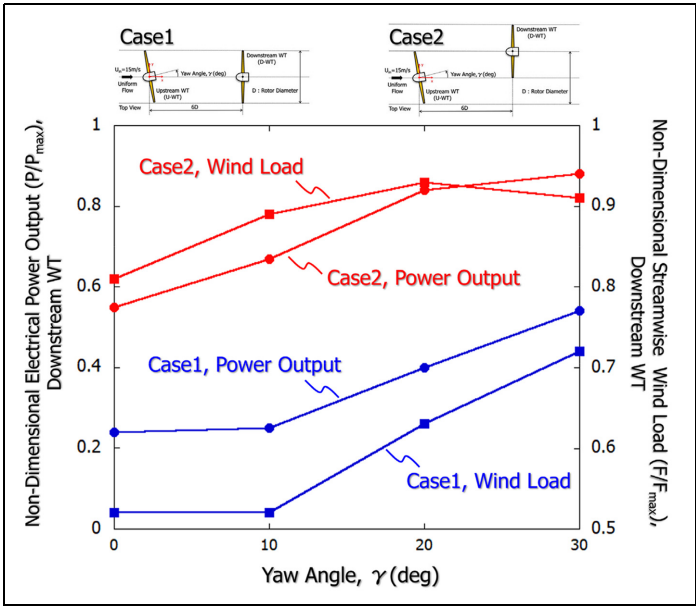
Figure 18 shows an example of the configuration and calibration of the load cell equipped with the downwind wind turbine model. Figure 19 shows the experimental setup of the wind load testing of the downwind wind turbine model in the Case 2. Figure 20 shows the maximum power output produced by the downwind wind turbine model in response to changes in the yaw angle of the upwind wind turbine model in the Case 2. Figure 20 also shows the streamwise wind load acting on the downwind wind turbine model at that time. The current measurements were repeated at least two to three times on different days and quantify the uncertainty in them. As a result, almost identical results were obtained without the need to draw error bars. Through careful observation of this figure, it can be seen that as the yaw angle of the upwind wind turbine model increased, the power output generated by the downwind wind turbine model and the wind load acting on it also increased. Due to the wake velocity deficits generated by the upwind wind turbine model, the wind velocity induced around the downwind wind turbine model is decreasing, so the streamwise wind load acting on the downwind wind turbine model did not exceed the stand-alone value. Also, the most interesting thing here is that the wind load in the Case 2 was considerably larger than that in the Case1. The main reason for this phenomenon is assumed to be that in Case 2, the downwind wind turbine model is partially affected by the wake flow generated by the upwind wind turbine model.

Figure 18. Configuration and calibration of load cell equipped with the downwind wind turbine model.

Figure 19. Experimental setup of the wind load testing of the downwind wind turbine model in the Case 2. Here, the Type-B model was used for both upwind and downwind wind turbines.

Figure 20. Maximum power output produced by the downwind wind turbine model in response to changes in the yaw angle of the upwind wind turbine and the streamwise wind load acting on the downwind wind turbine model in the Case 1 and the Case 2.

Conclusions

Power performance tests were initially conducted with a single rotor in isolation in order to characterize a rotor's power output in stand-alone conditions. In the current experiment, we obtained data for a total of seven cases with a yaw angle (γ) of 0° (non-yawed case) and yaw angles (γ) of 5°, 10°, 15°, 20°, 25°, and 30° (yawed cases). A detailed comparison of them revealed that the power output decreased rapidly as the yaw angle increased. It is presumed that the reason why the power output decreased in yawed cases is mainly the decrease in the effective rotor area and the change in the angle of the incoming wind flow with respect to the wind turbine blade. These facts result in inducing significant wake velocity deficits and inclined flows due to deflection of the wake behind the wind turbine. In the current experimental study, it was also clarified that the power output showed almost the same result regardless of the positive or negative yaw angle. Furthermore, through the examination of the effect of incoming wind speed on power output of Type-A model, it was shown that the power output of Type-A model also decreased as the incoming flow speed decreased, and the rotor rotation speed, which indicates the maximum value, also decreased.

The current work experimentally explored yawed wind turbine wake impacts on downwind wind turbine performances and streamwise wind loads for three different cases of merging wakes: (a) Case 1 ($y = 0$), (b) Case 2 ($y = 0.5D$), and (c) Case 3 ($y = 1D$), using two aligned wind turbine models with a rotor diameter (D) of 0.442 m and a height of 1 m ($= 2.26D$). The spacing between the upwind and the downwind wind turbine models was set to six times the diameter of the rotor (D) in all cases. Extremely large power output deficits of 46%–76% were seen in the Case 1. This is mainly due to the significant wake velocity deficits induced by the upwind wind turbine model. In the Case 2 with γ values of 20° and 30°, significant increases in the power output of the downwind wind turbines were observed, compared to a single wind turbine in isolation at the downwind wind turbine position (reference value). This result is considered to be mainly due to the upwind turbine-induced wake velocity deficits and wake deflection. Finally, in the Case 3, no significant difference was found in all results, and the tendency was almost the same. It was shown that the wake velocity deficits induced by the upwind wind turbine model and wake deflection had almost no effect on the power output of the downwind wind turbine model.

We evaluated the total power output of the two turbines. As a result, in the Case 2 with the yaw angle 20°, the total power output of the two wind turbine models was the highest due to the increase in the power output of the downwind wind turbine model. That is, the current experimental result demonstrated the wake steering effect when the upwind turbine model is yawed, and even though the upwind turbine model is expected to lose power by being yawed, the net power output can go up based on the increased power of downwind turbine model.

In order to consider the main cause of the significant increase in the power output of the downwind wind turbine model at the yaw angles 20° and 30° in the Case 2, we measured the lateral wind speed distribution at the $6D$ position on the downwind side of the upwind wind turbine model by using an ultrasonic anemometer. It was clarified that the peak of the wake velocity deficits induced by the upwind wind turbine model is clearly shifted away from the downwind turbine such that it experiences a smaller deficit due to wake steering. In addition, it was also clarified that the inclined flow was formed due to the deflection of the wake from the upwind wind turbine model.

Finally, for the downwind wind turbine model operating within the wake region induced by the upwind yawed wind turbine model, it is extremely important to understand the wind load acting on the downwind wind turbine model when the maximum power output was generated. Therefore, the downwind wind turbine model was mounted on a three-axis force measuring load cell, and the streamwise wind load acting on the turbine model was measured in the Case 2. It can be seen that as the yaw angle of the upwind wind turbine model increased, the power output generated by the downwind wind turbine model and the streamwise wind load acting on it also increased. However, it was also clarified that the streamwise wind load acting on the downwind wind turbine model in this situation did not exceed the stand-alone value. Additionally, the streamwise wind load in the Case 2 was considerably larger than that in the Case 1. The main reason for this phenomenon is assumed to be that in Case 2, the downwind wind turbine model is partially affected by the wake flow generated by the upwind wind turbine model.

Declaration of conflicting interests

Funding

ORCID iDs

Takanori Uchida (iD) https://orcid.org/0000-0003-2630-9113
Gustavo Richmond-Navarro (iD) https://orcid.org/0000-0001-5147-5952

Data availability

The data used to support the study are available from the corresponding authors upon request.

References

Barthelmie RJ, Pryor SC, Frandsen ST, et al. (2010) Quantifying the impact of wind turbine wakes on power output at offshore wind farms. *Journal of Atmospheric and Oceanic Technology* 27(8): 1302–1317.

Bartl J, Mühle F, Schottler J, et al. (2018) Wind tunnel experiments on wind turbine wakes in yaw: Effects of inflow turbulence and shear. *Wind Energy Science* 3(1): 329–343.

Bensason D, Simley E, Roberts O, et al. (2021) Evaluation of the potential for wake steering for US land-based wind power plants. *Journal of Renewable and Sustainable Energy* 13(3): 033303.

Brugger P, Debnath M, Scholbrock A, et al. (2020) Lidar measurements of yawed-wind-turbine wakes: Characterization and validation of analytical models. *Wind Energy Science* 5(4): 1253–1272.

Campagnolo F, Weber R, Schreiber J, et al. (2020) Wind tunnel testing of wake steering with dynamic wind direction changes. *Wind Energy Science* 5: 1273–1295.

Fleming P, Annoni J, Scholbrock A, et al. (2017) Full-scale field test of wake steering. *Journal of Physics Conference Series* 854(1): 012013

He R, Sun H, Gao X, et al. (2022) Wind tunnel tests for wind turbines: A state-of-the-art review. *Renewable and Sustainable Energy Reviews* 166: 112675.

Houck DR (2022) Review of wake management techniques for wind turbines. *Wind Energy* 25: 195–220.

Howland MF, Lele SK and Dabiri JO (2019) Wind farm power optimization through wake steering. *Proceedings of the National Academy of Sciences of the USA* 116(29): 14495–14500.

Kheirabadi AC and Nagamune R (2019) A quantitative review of wind farm control with the objective of wind farm power maximization. *Journal of Wind Engineering and Industrial Aerodynamics* 192: 45–73.

Li B, Zhou DL, Wang Y, et al. (2020) The design of a small lab-scale wind turbine model with high performance similarity to its utility-scale prototype. *Renewable Energy* 149(C): 435–444.

Lin M and Porté-Agel F (2019) Large-eddy simulation of yawed wind-turbine wakes: Comparisons with wind tunnel measurements and analytical wake models. *Energies* 12(23): 4574.

Matsumiya H, Kogaki T, Takahashi N, et al. (2011) Development and experimental verification of the new MEL airfoil series for wind turbines. *Proceedings of Japan Wind Energy Symposium* 22: 92–95.

Miao W, Li C, Yang J, et al. (2016) Numerical investigation of the yawed wake and its effects on the downstream wind turbine. *Journal of Renewable and Sustainable Energy* 8(3): 033303.

Porté-Agel F, Bastankhah M and Shamsoddin S (2020) Wind-turbine and wind-farm flows: A review. *Boundary-Layer Meteorology* 174(1): 1–59.

Qian GW and Ishihara T (2018) A new analytical wake model for yawed wind turbines. *Energies* 11(3): 665.

Richmond-Navarro G, Uchida T and Calderón-Muñoz WR (2021) Shrouded wind turbine performance in yawed turbulent flow conditions. *Wind Engineering* 46(2): 518–528.

Schottler J, Bartl J, Mühle F, et al. (2018) Wind tunnel experiments on wind turbine wakes in yaw: Redefining the wake width. *Wind Energy Science* 3(1): 257–273.

Wei DZ, Wang NN and Wan DC (2021) Modelling yawed wind turbine wakes: Extension of a Gaussian-based wake model. *Energies* 14(15): 4494.